LAWRENCE
LIVERMORE
NATIONAL
LABORATORY

UCRL-JRNL-233964

Quantifying the effects of three-dimensional subsurface heterogeneity on Hortonian runoff processes using a fully-coupled numerical, stochastic approach.

Reed M Maxwell, Stefan J Kollet

August 24, 2007

Advances in Water Resources

Quantifying the effects of three-dimensional subsurface heterogeneity on Hortonian runoff processes using a fully-coupled numerical, stochastic approach.

Reed M. Maxwell and Stefan J. Kollet*

Atmospheric, Earth and Energy Sciences Department, Lawrence Livermore National Laboratory, Livermore, CA, USA

**Current Address: Meteorological Institute, Bonn University, Germany*

Aug 23, 2007

Abstract

The impact of three-dimensional subsurface heterogeneity on hillslope runoff generated by excess infiltration (so called Hortonian runoff) is examined. A fully-coupled, parallel subsurface overland flow model is used to simulate runoff from an idealized hillslope. Ensembles of correlated, Gaussian random fields of saturated hydraulic conductivity are used to create uncertainty and variability (i.e. structure) due to subsurface heterogeneity. A large number of cases are simulated in a parametric manner with variance of the hydraulic conductivity varied over two orders of magnitude. These cases include rainfall rates above, equal and below the geometric mean of the hydraulic conductivity distribution. These cases are also compared to theoretical considerations of runoff production based on simple assumptions regarding (1) the rainfall rate and the value of hydraulic conductivity in the surface cell using a spatially-indiscriminant approach; and (2) a percolation-theory type approach to incorporate so-called runon. Simulations to test the ergodicity of hydraulic conductivity on hillslope runoff are also performed. Results show three-dimensional features (particularly in the vertical dimension) in the hydraulic conductivity distributions that create shallow perching, which has an important

25 effect on runoff behavior that is fundamentally different in character than previous two
26 dimensional analyses. The simple theories are shown to be very poor predictors of the saturated
27 area that might runoff due to excess infiltration. It is also shown that ergodicity is reached only
28 for a large number of integral scales (~30) and not for cases where the rainfall rate is less than
29 the geometric mean of the saturated hydraulic conductivity.
30
31 **Introduction and Background**
32 There has been interest and need to understand the role of the subsurface heterogeneity in
33 the processes of overland flow runoff generation. Though the role of heterogeneity has been
34 investigated in previous studies (e.g. Woolhiser et al, 1996), in the processes of runoff and re-
35 infiltration of overland flow (so-called runon), the interactions between the uncertainty in spatial
36 variability in saturated hydraulic conductivity, K_s, and the ensuing impact on runoff processes
37 have not been greatly explored. Two recent papers by Nahar et al. (2004) and Herbst et al.
38 (2006) have addressed these concepts and, in addition, comprehensively summarized the pre-
39 existing literature. Therefore only studies dealing with coupled subsurface and overland flow
40 using stochastic representations will be discussed here.
41 Perhaps the first study to look at coupled surface-subsurface flow utilizing a stochastic
42 representation of K_s was Binley et al. (1989). They simulated three dimensional subsurface
43 random fields of K_s using a correlated, Gaussian approach and demonstrated its impact on
44 overland flow due to excess infiltration and excess saturation. They looked at different cases
45 with different parameter vales but performed a limited number of simulations due to the
46 computational constraints at that time.
47 Nahar et al (2004) used an overland flow formulation with an analytical, single-column
48 subsurface infiltration model to investigate field-scale infiltration caused by runon (downslope

49 re-infiltration of runoff due to an increase in K_s) using two dimensional, correlated random fields
50 to simulate subsurface properties. They showed the importance of runon on subsurface recharge.
51 They also presented a non-dimensional framework and investigated the uncertainty in spatial
52 distribution of K_s using a Monte Carlo approach for some cases over a modest range of
53 parameter values. Using this approach they showed that for rainfall rates lower than the mean
54 hydraulic conductivity outflow increases with increasing heterogeneity (increasing variance in
55 K_s) but found this relationship reversed for greater rainfall rates.

56 Herbst et al (2006) applied a three dimensional hydrologic model to a small catchment.
57 They looked at five different representations of subsurface heterogeneity and compared the
58 hydrologic model results to the actual system. They found that a conditional stochastic approach
59 best represented the conditions of the real system.

60 Though primarily focused on theoretical surface-subsurface coupled model development,
61 Kollet and Maxwell (2006) investigated the effects of correlated, random fields of K_s on overland
62 flow in a two-dimensional (vertical) test case. Using a small number of realizations this work
63 showed how shallow perching, runoff, runon and infiltration interact simultaneously to affect
64 hillslope outflow.

65 These previous studies all point to the need for an investigation of these processes and
66 their interactions in a more systematic manner. In the current study, we apply a novel, fully
67 coupled surface-subsurface flow model to investigate the effects of three-dimensional
68 heterogeneity in K_s on overland flow using a comprehensive set of simulations. These
69 simulations are designed to address the following four questions:

70 1. How does three-dimensional subsurface heterogeneity influence (transient)
71 outflow rates and their variability?

2. What is the fraction of saturated area for a certain rainfall rate and can we use estimates of this fraction to deduce average outflow rates (or vice versa)?
3. Does a two-dimensional representation of subsurface heterogeneity suffice or is a three-dimensional representation necessary to capture accurately runoff processes?
4. Does the concept of ergodicity apply? That is, how large does a hillslope have to be, with regard to the scale of the heterogeneity, to exhibit effective behavior?

In order to address these questions, we perform a large number of numerical experiments. These experiments include a wide range of parameter values with a variance of K_s spanning two orders of magnitude. Additionally, we simulate three dimensional structure in the subsurface heterogeneity and ergodic domains, both features not previously investigated. First, the coupled modeling approach is presented; next, non-dimensional parameters are introduced; and third, the case studies, including a table of parameter values, are detailed. Finally, the results of the simulations are presented and discussed along with implications for field scale runoff.

Coupled Model

In this study, we use the flow code ParFlow to simulate fully-coupled surface and subsurface flow via an overland flow boundary condition. While complete details of this approach are given in Kollet and Maxwell (2006), a brief summary of the equations are presented below. ParFlow solves the Richards' equation in three spatial dimensions which may be written as:

$$S_s S_w \frac{\partial \psi_p}{\partial t} + \phi \frac{\partial S_w(\psi_p)}{\partial t} = \nabla \cdot \mathrm{q} + q_s \qquad (1)$$

$$\mathrm{q} = -K_s(x)k_r(\psi_p)\nabla(\psi_p - z)$$

where ψ_p is the subsurface pressure head [L], z is depth below the surface [L], $K_s(x)$ is the saturated hydraulic conductivity [LT^{-1}], k_r is the relative permeability [-] (a function of pressure head, ψ_p), S_s is the specific storage coefficient [L^{-1}], ϕ is the porosity [-], S_w is the degree of saturation [-] and q_s is the general source/sink term [T^{-1}].

Shallow overland flow is represented in ParFlow by the two-dimensional kinematic wave equation, which appears in the overland flow boundary condition after applying continuity conditions of pressure and flux:

$$-K_s(x)k_r(h-z) = \frac{\partial \|h_s,0\|}{\partial t} - \nabla\vec{v}\|h_s,0\| + q_r(x) \qquad (2)$$

where $\vec{v}$ is the depth averaged velocity vector [LT^{-1}]; h_s is the surface ponding depth [L] and $q_r(x)$ is the a general source/sink (e.g. rainfall) rate [LT^{-1}]. Note that $\|h_s,0\|$ indicates the greater value of the two quantities and that the overland flow condition assumes that $h_s = \Psi_p$ at the ground surface under saturated conditions (Kollet and Maxwell, 2006). If diffusion terms are neglected the momentum equation can be written as

$$S_{f,i} = S_{o,i} \qquad (3)$$

which is commonly referred to as the kinematic wave approximation. In Equation 3 $S_{o,i}$ is the bed slope (gravity forcing term) [-], which is equal to the friction slope $S_{f,i}$ [L]; i stands for the x- and y-direction.

Manning's equation is used to establish a flow depth-discharge relationship

$$\mathrm{v}_x = -\frac{\sqrt{S_{f,x}}}{n} h_s^{2/3} \text{ and } \mathrm{v}_y = \frac{\sqrt{S_{f,y}}}{n} h_s^{2/3} \qquad (4)$$

where n [$TL^{-1/3}$] is the Manning's coefficient.

ParFlow additionally has the ability to represent the hydraulic conductivity distribution of the subsurface as a correlated, space random field using a parallel, Turning Bands approach (Tompson et al 1989; Ashby and Falgout, 1996; Tompson et al 1998). To incorporate this feature, we choose to represent the spatial variation of hydraulic conductivity as a statistically stationary, random field where:

$$\ln K(\mathbf{x}) = F + f(\mathbf{x}) \quad (5)$$

and $\overline{\ln K(x)} = F$, $\overline{f(x)} = 0$ with $\overline{f(x)^2} = \sigma_f^2 = \sigma_{\ln K}^2$ and $K_g = e^F$. The mean or expected value of the *ln*K is signified by the overbar and K_G is the geometric mean of the hydraulic conductivity. The correlation of any two hydraulic conductivity values separated by a distance, ξ, with a correlation scale, λ, is represented by an exponential of the form:

$$R_{ff}^e(\xi) = \sigma_f^2 e^{-\xi/\lambda} \quad (6).$$

Note that the correlation scale, λ, in (6) is equivalent to the integral scale, I (see section 2.3.1 in Rubin, 2003). While this technique of representing spatially correlated heterogeneity has been widely applied in subsurface flow (e.g., Smith and Schwartz, 1980; Dagan, 1989; Tompson and Gelhar, 1990; Rubin and Dagan, 1992) it is an approximate description of the subsurface heterogeneity usually applied at smaller spatial scales (e.g. Carle and Fogg, 1996; Carle and Fogg, 1997; Tompson et al, 1998).

Non-dimensionalization of the governing equations.

First, we introduce the rain application time, t_a and the length of the hillslope, L, in the direction of overland flow. We are interested in the relationship between the rainfall rate and the ability of the subsurface to infiltrate this rainfall. It is common to think about the rainfall rate, Q_{rain}, in relation to the saturated hydraulic conductivity of the subsurface, K_s. However, we are

using a correlated, space-random field to simulate the subsurface heterogeneity in K_s, therefore we choose to non-dimensionalize Q_{rain} by the geometric mean of the hydraulic conductivity

$$q_r` = \frac{Q_{rain}}{K_g} \quad (7).$$

It is then natural to transform saturated hydraulic conductivity in the same manner, as

$$K` = \frac{K_s}{K_g} \quad (8).$$

We may then combine saturation and porosity:

$$S` = \phi S \quad (9).$$

As we are interested in non-dimensionalizing with respect to the length scales of heterogeneity, we define L in terms of integral scales, I_x=I_y:

$$x` = \frac{x}{L} = \frac{x}{I_{x,y}} \quad (10), \text{ and}$$

$$z` = \frac{z}{L} = \frac{z}{I_{x,y}} \quad (11).$$

As stated earlier, we define time in terms of application time of the rainfall, t_a:

$$t` = \frac{t}{t_a} \quad (12).$$

This results in the following parameter groupings for the soil pressure head and ponding depth:

$$h` = \frac{h}{K_g t_a} \quad (13),$$

and the velocity:

$$v` = \frac{vt_a}{L} = \frac{vt_a}{I_{x,y}} \quad 14).$$

The governing equations, then become:

156 $$\frac{\partial S`}{\partial t`} = \nabla \cdot \left[k` k_r \nabla \left( h` - z` \right) \right] \quad (15)$$

157 $$- k` k_r \nabla \left( h` - z` \right) = \frac{\partial \left\| h`, 0 \right\|}{\partial t`} - \nabla \mathrm{v}` \left\| h`, 0 \right\| - q`_r \quad (16).$$

158

159 **Problem Setup**

160 To investigate the effects of three-dimensional subsurface heterogeneity on Hortonian
161 hillslope runoff, we employ the numerical experiment shown in Figure 1. The experiment
162 consists of a uniform hillslope that terminates at a perpendicular channel. Water may exit the
163 hillslope anywhere along the channel though flow in the channel is not explicitly simulated. The
164 domain size is 6x6 integral scales and the lateral grid dimensions are nx=ny=30 and $\Delta x` = \Delta y` = 0.2$
165 $I_{x,y}$. We use a fine vertical discretization with nz=150 (for 135,000 compute cells) and $\Delta z` =$
166 $0.0004\ I_{x,y}$, (or $0.04\ I_z$) for a default domain size 6 I_z deep, to insure accurate solutions of surface-
167 subsurface interactions. The friction slopes are constant in the *x*- and *y*-direction $S_{fx}=0$, $S_{fy}=-$
168 0.005 with a constant manning's roughness coefficient of 2.9×10^{-6} ($t_d / I_{x,y}^{1/3}$). Rain is applied
169 uniformly over the entire hillslope for $\Delta t' = 1$ with an ensuing recession of an additional $\Delta t' = 1$
170 resulting in a total simulation time of $t' = 2$. To ensure Hortonian conditions, the water table is
171 initialized at the bottom of the domain resulting in an initial hydrostatic pressure distribution
172 with dry conditions at the ground surface.

173 The numerical experiments are designed to directly address the four questions posed
174 earlier. For the complete set of numerical experiments, we systematically change the variance of
175 the hydraulic conductivity field, $\sigma^2_{\ln K}$, (i.e. the degree of subsurface heterogeneity), the
176 normalized rainfall rate, the statistical anisotropy and the size of the domain.

For the base-case, we performed a series of simulations using statistically anisotropic fields with $\varepsilon = I_z/I_{x,y} = 0.01$ (as defined in Rubin, 2003 and Dagan, 1989). The results of these simulations are used to quantify the influence of subsurface heterogeneity on outflow rates and to study the relationship of fraction of saturated area and outflow rate. Additionally, statistically isotropic simulations were performed and compared to the anisotropic simulations to examine whether a two-dimensional representation of subsurface heterogeneity suffices to capture the main processes of runoff production. We simulate 50 realizations of hydraulic conductivity distribution for each case and average all results over this ensemble. Each realization was generated using a parallel version of the turning bands algorithm (Tompson et al, 1989) utilizing 75 lines, $r_\zeta = 5.0$ and $\Delta k = 0.2$.

Additionally, we simulated six ergodic cases that are $72 I_x$ wide consisting of a single realization. Again, we use a parallel version of the turning bands algorithm utilizing 350 lines, $r_\zeta = 5.0$ and $\Delta k = 0.2$. This set of simulations examines the average behavior of a hillslope, which is of great significance with regard to upscaling. In summary, we simulate 33 different cases including 1,209 different individual simulations. All simulations and associated parameters are shown in Table 1.

Figure 2 displays the five lognormal distributions of hydraulic conductivity used in these numerical simulations, normalized by the rainfall rate. This figure also delineates the three non-dimensional rainfall rates used in this study. Inspection of this figure provides some indication of expected runoff behavior; for example, simulations using the intermediate rainfall rate should show very little sensitivity to $\sigma^2_{\ln K}$.

201 Table 1. List of all numerical simulations and parameter values.

Simulations	$\sigma^2_{\ln K}$	Q_{rain}/K_g	ε	L_x	Number of realizations
Anisotropic (base case)	0.1	0.5	0.01	6	50
	0.5				
	1				
	5				
	10				
	0.1	1.0			
	0.5				
	1				
	5				
	10				
	0.1	2			
	0.5				
	1				
	5				
	10				
Isotropic	1	0.5	1		
	0.5				
	5				
	1	1.0			
	0.5				
	5				
	1	2			
	0.5				
	5				
Ergodic	0.5	1	0.1	72	1
	1.0				
	5				
	0.5	0.5			
	1.0				
	5				
	0.5	2			
	1.0				
	5				

202

203

204

205

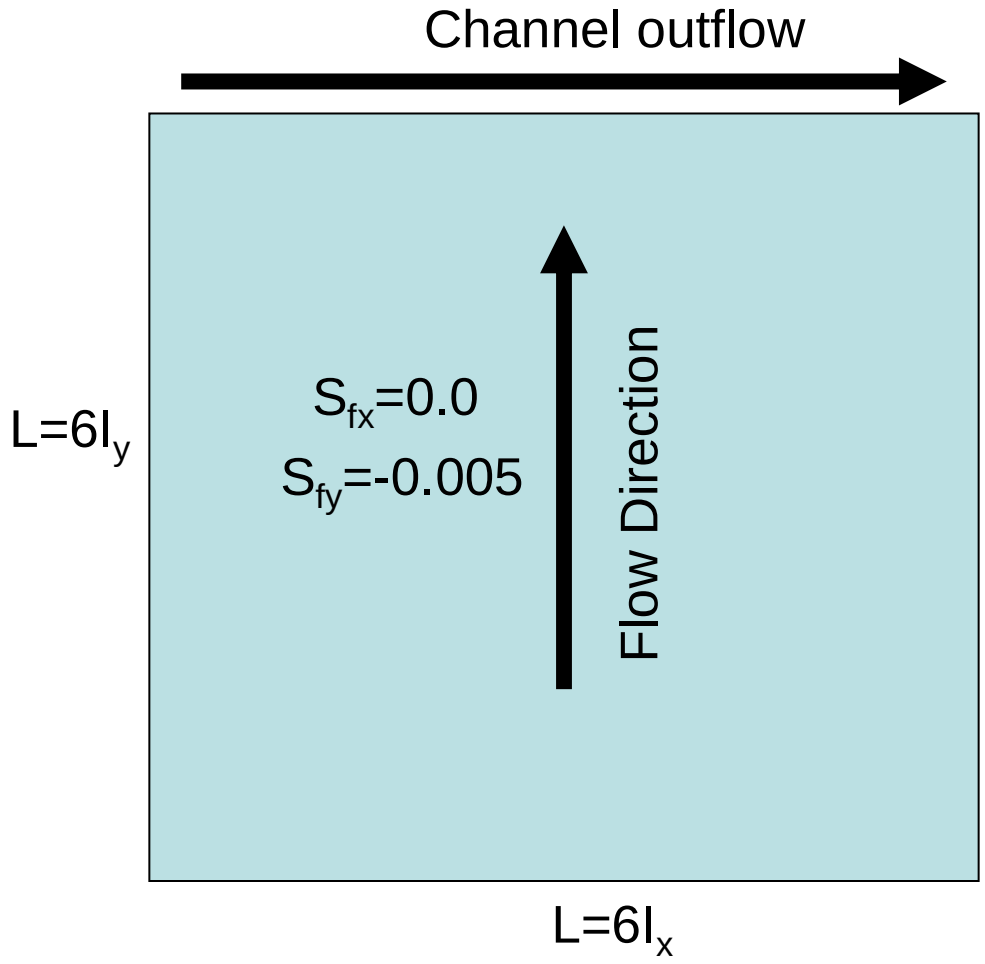

206

207 Figure 1. Problem setup and schematic.

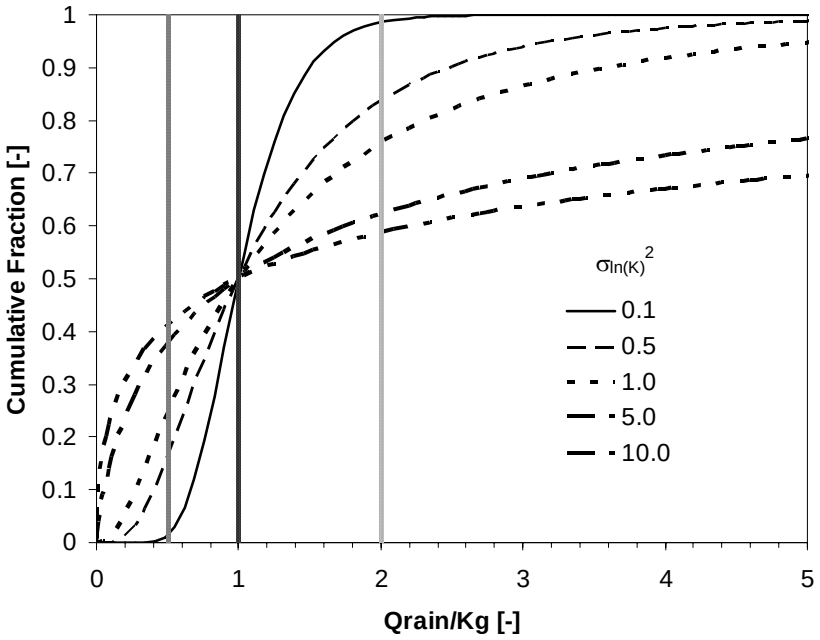

Figure 2. Plot of cumulative, lognormal distributions for the five variances used in this study, normalized as a function of rainfall rate over the geometric mean of hydraulic conductivity. The three normalized rainfall rates are also plotted on this figure as gray, vertical lines.

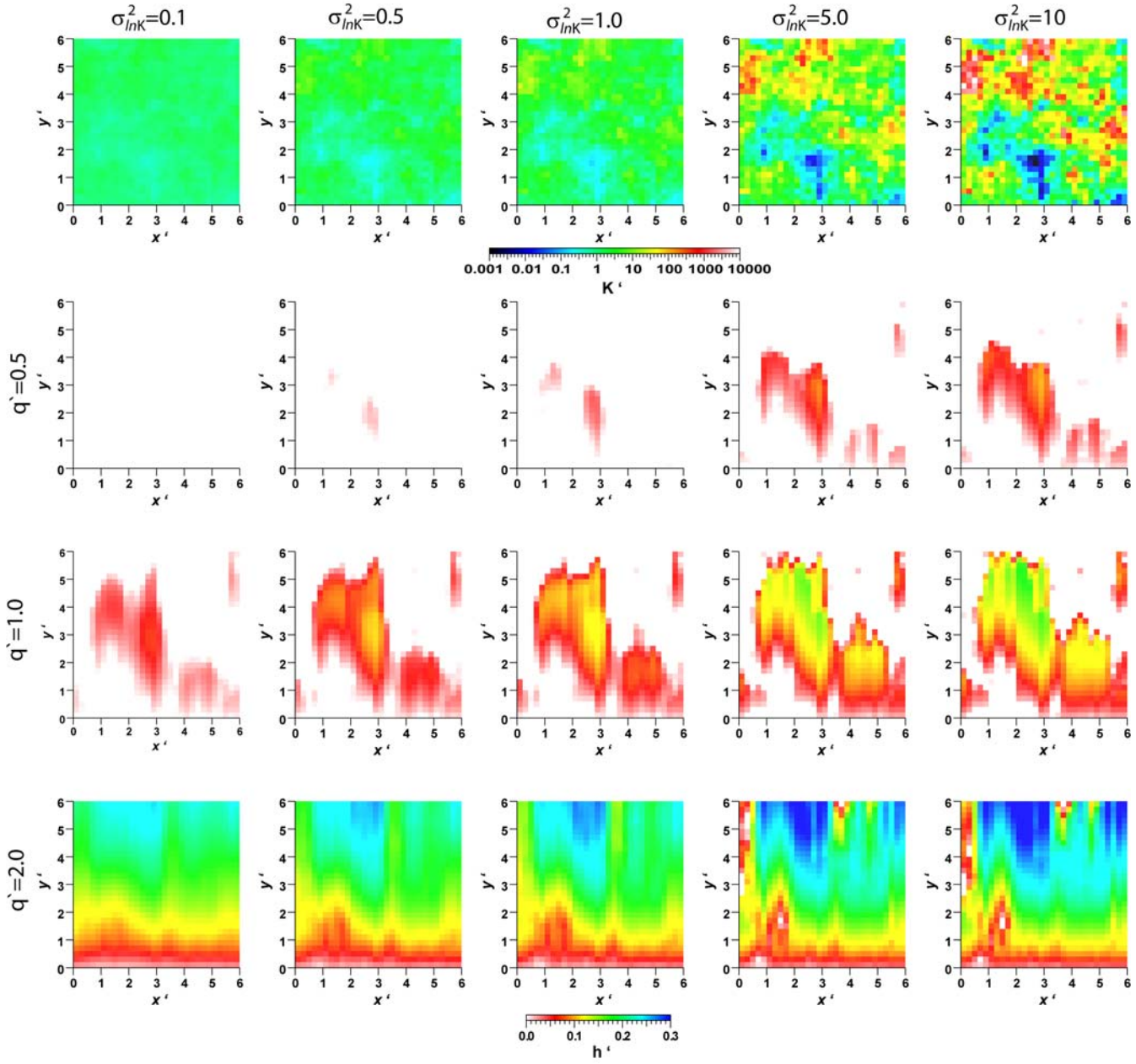

Figure 3. Plot of non-dimensional hydraulic conductivity (*K`*) at the land surface (top) for a range of increasing variances of *ln*K from left to right as shown for a single realization, 20. Next three rows are plots of non-dimensional depth of ponded water (*h`*) for these corresponding realizations at t`=1 for increasing non-dimensional rainfall rates q`=0.5, 1.0 and 2.0. Note outflow occurs at the top of each panel.

Results and Discussion

Figure 3 plots a single realization of hydraulic conductivity field for the range of $\sigma^2_{\ln K}$ simulated in this work. All plots are for the same random seed (and thus the same spatial pattern of heterogeneity), with $\sigma^2_{\ln K}$ increasing from left to right. Also shown in the figure are the corresponding depths of ponded water at $t^{`}$=1, the time of peak flow. These plots are for cases of increasing Q_{rain} from top to bottom. These plots illustrate the increase in ponding depth both with increasing rainfall (top to bottom Figure 3) and increasing heterogeneity (left to right, Figure 3).

Figure 4 plots the non-dimensional hydrograph, averaged over all realizations for the base-case simulations; that is for five $\sigma^2_{\ln K}$ and three non-dimensional rainfall rates. In this figure we see an increase in outflow with increasing $\sigma^2_{\ln K}$ for all three rainfall rates. This increase is most significant for the lowest rainfall rate and least significant for the highest rainfall rate.

Figure 5 summarizes this information, plotting the total, non-dimensional outflow as a function of $\sigma^2_{\ln K}$ for the three rainfall rates. This figure plots the ensemble average outflow over all realizations (solid line) and the average +/- one standard deviation of outflow (dashed lines). In this figure, we again see an increase in percent total outflow with increasing $\sigma^2_{\ln K}$. There is also an increasing variance in the outflow rate (generated by the difference in outflow from different realizations of hydraulic conductivity) with increasing $\sigma^2_{\ln K}$.

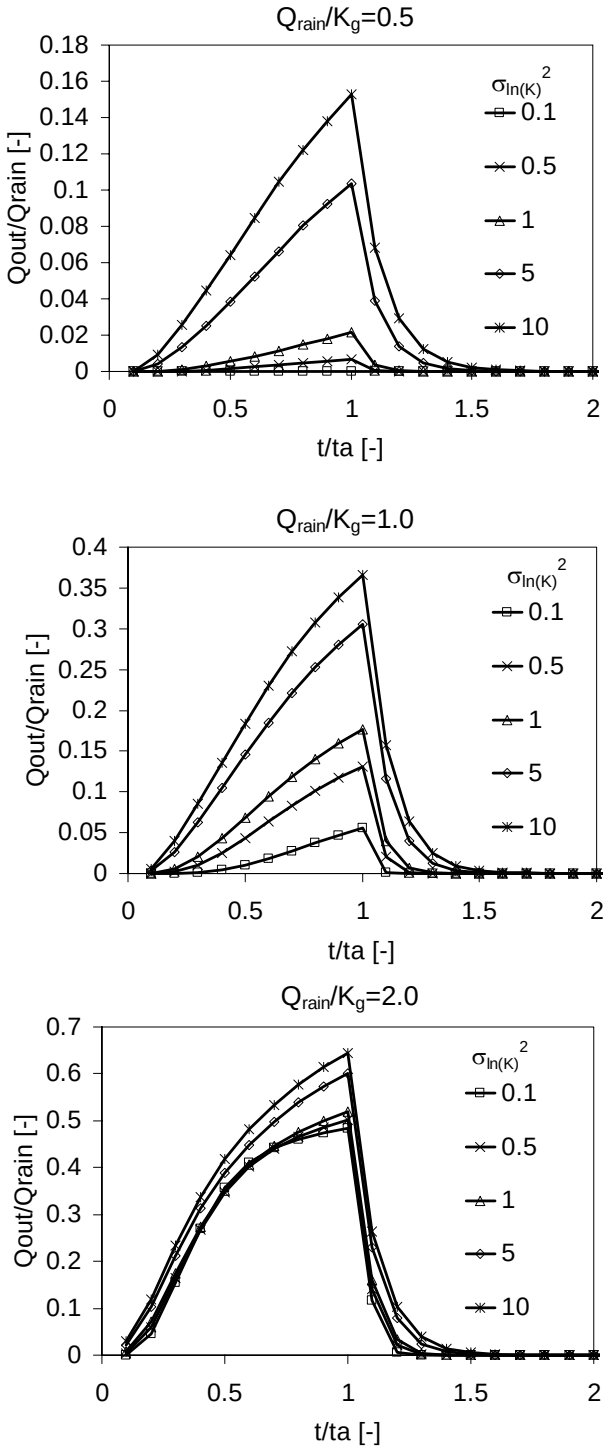

Figure 4. Plot of the ensemble average of non-dimensional outflow against non-dimensional time for five values of variance of ln(K) (different symbols as noted) for three non-dimensional rainfall rates, as labeled, increasing in amount from the top panel to the bottom panel. Note the different scale for the y-axis in the three panels of this figure.

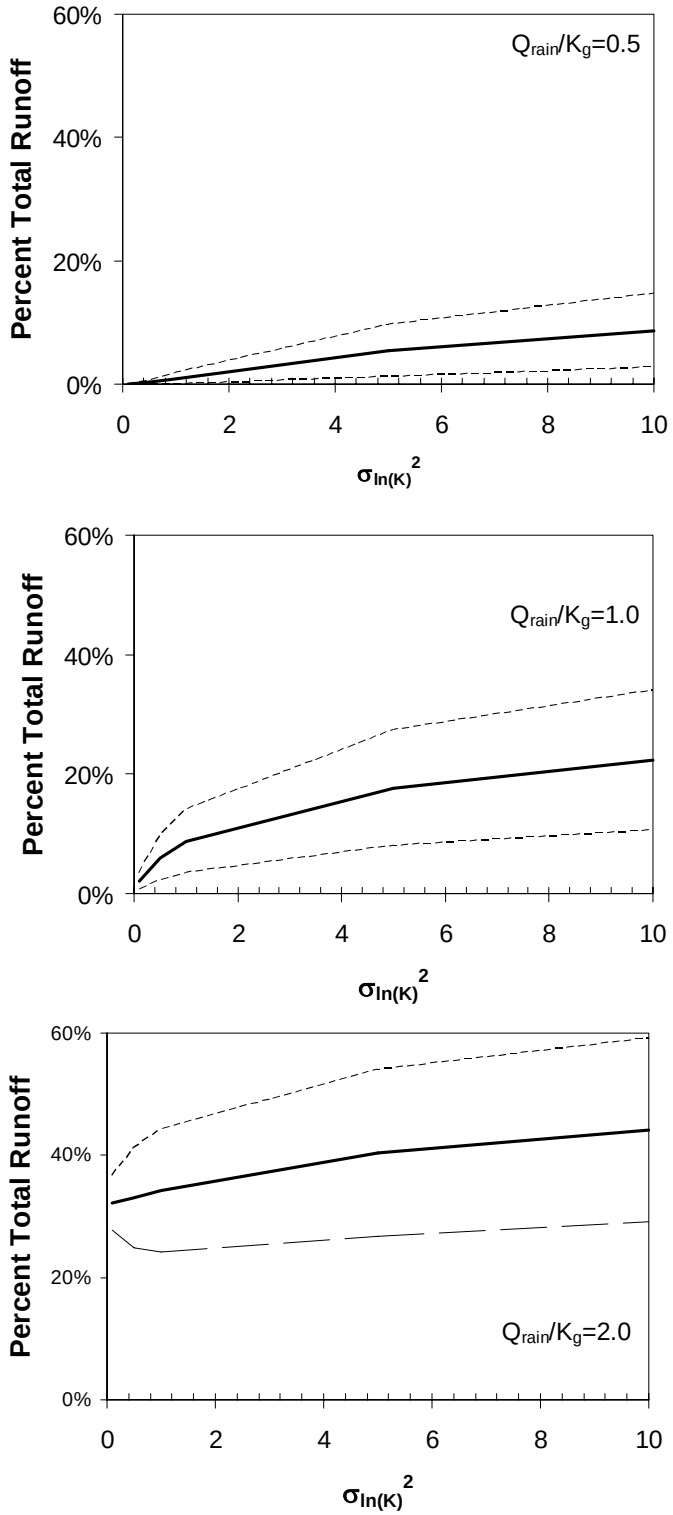

Figure 5. Plot of percent total runoff as a function of variance of ln(K) for the three non-dimensional rainfall rates simulated. The average over all realizations is plotted as the solid line while the average +/- one standard deviation is plotted as the dashed lines.

250

251 At the ground surface, the fractional saturated area (cells with $S_w \geq 1$ and $\psi \geq 0$) was
252 calculated at $t^{`}$=1 (time of peak flow) for all $\sigma^2_{\ln K}$ values and rainfall rates in two distinct ways.
253 First, the fractional area was calculated, regardless of connection to the channel, i.e. any
254 saturated area was counted regardless of spatial orientation. In the second approach, only those
255 cells were counted that provided a contiguous or connected saturated path to the channel. The
256 calculated fractional saturated areas were then averaged over all realizations. Figure 6 plots the
257 results of this calculation, fraction of saturated area, total and connected, as a function of $\sigma^2_{\ln K}$
258 for the three rainfall rates. In this figure we see that for the lowest rainfall rate (Q_{rain}/K_g=0.5, left
259 panel) the fraction of saturated area increases with increasing $\sigma^2_{\ln K}$. This is also the case for the
260 Q_{rain}/K_g=1.0 case (middle panel) though there is less of an increase for larger $\sigma^2_{\ln K}$. For the
261 largest rainfall rate (Q_{rain}/K_g=2.0) we see the opposite relationship; decreasing fractional
262 saturated area with increasing $\sigma^2_{\ln K}$.

263 In Hortonian overland flow, one may attempt to calculate the fraction of ponded, or
264 saturated surface cells based on the shape of the assumed distribution of *ln*(K) and the rainfall
265 rate. This may be done in two ways, one that does not take into account the lateral spatial
266 structure of the saturated hydraulic conductivity field and one that does and accounts for both
267 runoff and runon processes. For the former case, the fraction of saturated area may be calculated
268 as the fraction of the distribution of *ln*(K) that is less than the rainfall rate. This may be viewed
269 graphically as the intersection of the rainfall values and the distribution of *ln*(K) shown in Figure
270 2. This approach is similar in concept to runoff parameterizations in many classes of land
271 surface models (e.g. Wetzel et al, 1996; Liang et al, 1996; Lohmann et al, 1998). For the latter,
272 connected case, the lateral spatial distribution saturated hydraulic conductivity affects the

273 calculation. In this case, the fraction of saturated hydraulic conductivity values below the
274 rainfall rate, connected to the channel (starting at the outflow side of the hillslope and working
275 upward) were calculated from the generated random fields and then averaged. These calculations
276 were performed for both cases are plotted as a function of rainfall rate and variance as the heavy
277 solid (total) and dashed lines (connected) in Figure 6.

278 We see, in Figure 6, that the fractional surface saturated areas calculated from the
279 distributions of hydraulic conductivity almost always under-predict the simulated values. Only
280 at the smallest variance of 0.1 do the fractional surface saturations agree and the most
281 pronounced differences are for values of $\sigma^2_{\ln K}$ greater than one. The largest difference (50%) in
282 the predicted and simulated fractional saturated surface area is for the rainfall rate of
283 Q_{rain}/K_g=1.0. At this rainfall value, the fractional surface areas calculated from the distribution
284 of *ln*(K) predict no change with variance of *ln*(K). The simulated values show that this not the
285 case and suggest that consideration of other processes is important, which are discussed below.

286 There are two physical processes accounted for in the simulations that create the
287 differences seen in Figure 6. These processes are runon-generated excess infiltration and
288 shallow perched or ponded zones. Runon generated excess infiltration occurs when the saturated
289 hydraulic conductivity of a tile is greater than the rainfall rate but not greater than the sum of the
290 rainfall rate and the inflow from an upslope tile that is already saturated and generating runoff.
291 This is a variation of the runon process but instead of the runon water leading to subsurface
292 infiltration as simulated by previous studies, it may still run off later from a downslope tile, given
293 these conditions.

294 Shallow perching is ponded water that builds up at the land surface (and runs off) not due
295 to the surface value of hydraulic conductivity being lower than the rainfall rate but due to low-*K*
296 values just below the land surface. This water initially infiltrates but eventually cannot flow past

297 a low-*K* layer in the shallow subsurface and saturates the cells above this low-*K* cell and
298 eventually ponds water at the land surface which then runs off. An example of this phenomenon,
299 as simulated by the coupled model, may be seen in Figure 13 of Kollet and Maxwell (2006). It is
300 clear from Figure 6 that both these processes are occurring and important, particularly at large
301 $\sigma^2_{\ln K}$.
302

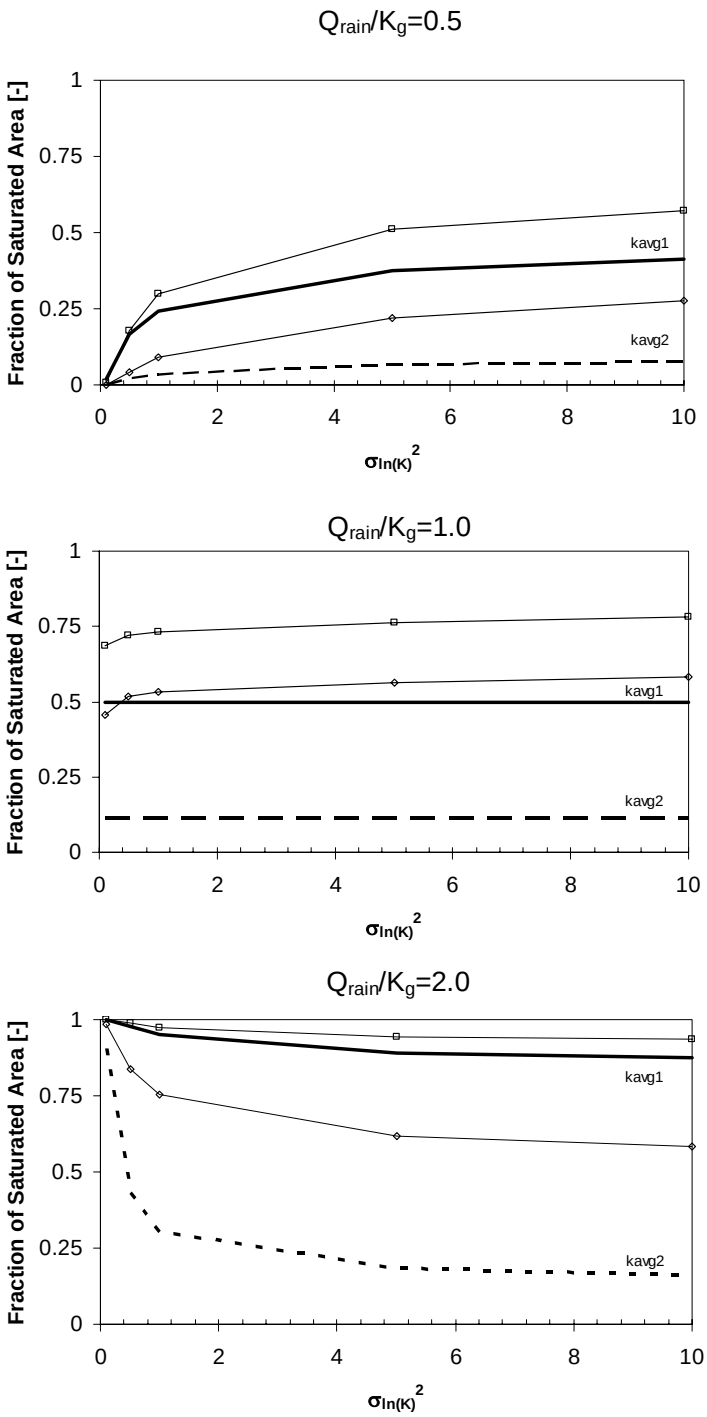

303

304 Figure 6. Plot of calculated fractional total (thin lines with squares) and connected (thin lines with diamonds)

305 saturated area at t' = 1, averaged over all realizations, as a function of variance of ln(K) for the three rainfall rates.

306 The fractional areas predicted by the distribution of hydraulic conductivity that is less than the rainfall rate is also

307 shown for total (k_{avg1},heavy solid line) and connected (k_{avg2}, dashed line).

308

309 The ergodicity of heterogeneous hillslope processes have not been previously
310 investigated. Ergodicity has, however, been a common topic in other areas such as subsurface
311 transport (e.g. Dagan, 1989; Rubin, 2003) and is defined as the equivalence between spatial and
312 ensemble statistics (Rubin, 2003). The condition of ergodicity plays an important role in
313 understanding when a hillslope is of sufficient spatial scale that effective behavior would be
314 expected. Therefore, understanding of ergodicity is key in upscaling subgrid heterogeneity to
315 simulate runoff processes in large scale models.
316 In order to examine ergodicity, a series of very large (72 Integral scales wide) domains
317 were constructed for three $\sigma^2_{\ln K}$ values, 0.5, 1.0 and 5.0, for the three rainfall rates. The
318 cumulative outflow was calculated and normalized for increasing distances (and thus
319 corresponding hillslope areas) along the channel (i.e. the *x*-axis). In this way, not only the total
320 fractional outflow, but the fractional outflows for domain widths ranging from 0.2 to $72I_x$ could
321 be calculated as well. These outflows are plotted in Figure 7 as a function of non-dimensional
322 catchment width for the three values of $\sigma^2_{\ln K}$ and for the three rainfall rates (solid curves). For
323 each plot, the corresponding ensemble average of total fractional outflow was also plotted
324 (dashed curves). Comparison of these two curves (and particularly their intersection) provides
325 an estimate of the catchment width needed for ergodic behavior of Hortonian runoff.
326 Inspection of the curves in Figure 7 demonstrates several important features. One, the
327 total outflow again increases both with increasing $\sigma^2_{\ln K}$ and with increasing rainfall rate.
328 Additionally, for lower variances ($\sigma^2_{\ln K}$=0.5 and 1.0) and for the lowest rainfall rate, ergodic
329 behavior with catchments narrower than $72I_x$ is unlikely. For the two larger rainfall rates,
330 ergodic behavior is approached at catchments approximately 30 integral scales wide with a
331 smoother transition to ergodic behavior at the largest rainfall rate.

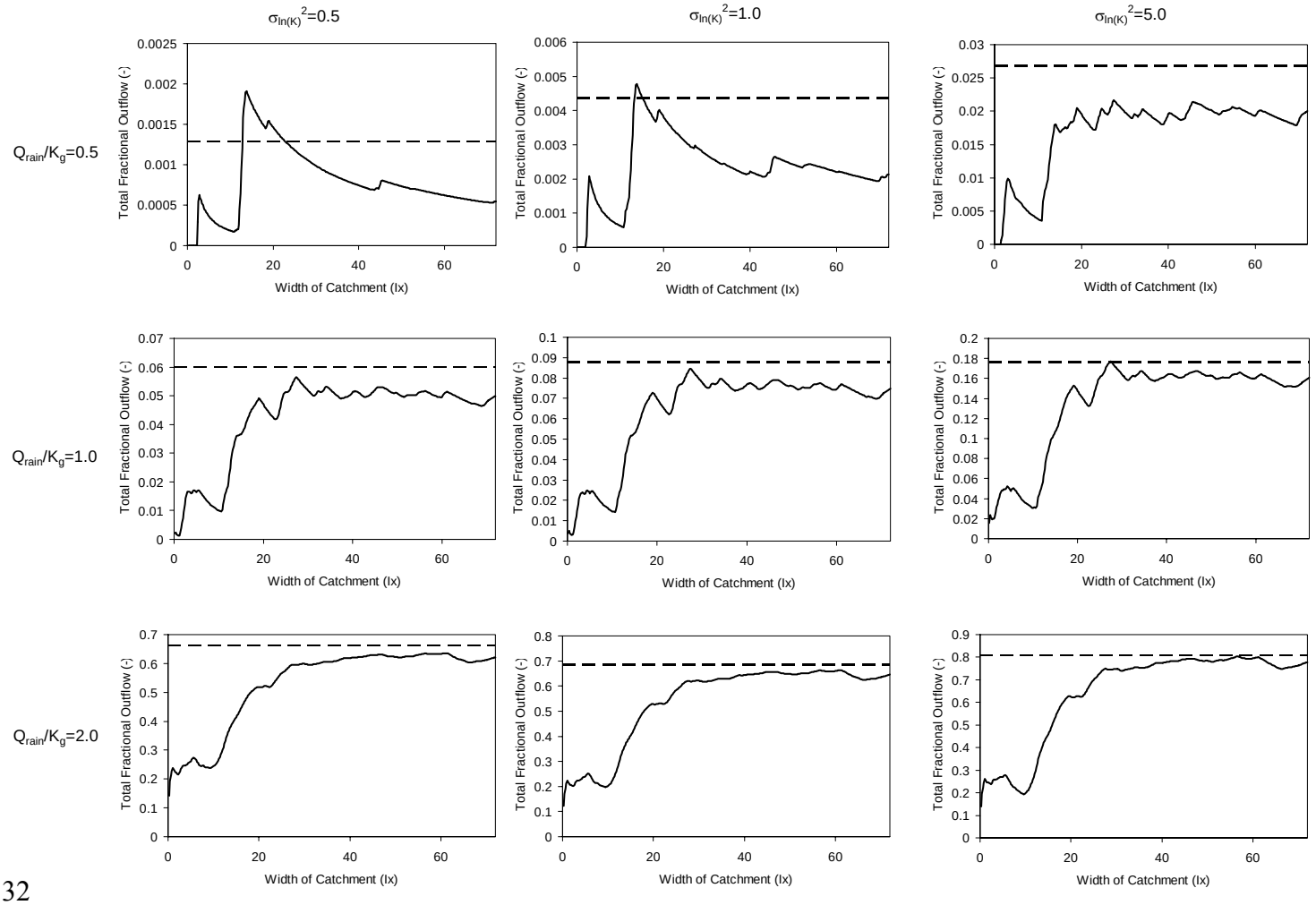

Figure 7. Plot of total fractional outflow as a function of increasing catchment width for a large, single realization of hydraulic conductivity (solid line), for three variances of ln(K) (left to right) and for increasing non-dimensional rainfall rate (top to bottom). The ensemble average of total fractional outflow (as in Figure 5) is plotted as the horizontal, dashed line. Note the different y-axis for each panel in this figure.

The trends seen in Figures 4 and 5 that outflow always increases with increasing $\sigma^2_{\ln K}$, are somewhat counterintuitive, particularly at the larger rainfall rates. Additionally, these trends do not agree with the findings of Nahar et al (2004). The work of Nahar and colleagues was more simplified than the current study and among other aspects, only considered two-dimensional random fields of hydraulic conductivity and did not fully couple the surface and subsurface in

343 the same manner done in the current work. Though they include the important process of runon
344 in their analysis, their results do not honor processes related to runon-generated excess
345 infiltration and additional processes resulting from vertical heterogeneity in the hydraulic
346 conductivity, such as perching in the shallow subsurface. To investigate the importance of
347 vertical structure in hydraulic conductivity and processes related to shallow perching a series of
348 simulations with a much larger statistical anisotropy ratio, ε=1, were simulated and compared to
349 the base-case simulations with ε=0.01 for $\sigma^2_{\ln K}$ = 0.5, 1.0 and 5.0. Though still generated with a
350 three-dimensional hydraulic conductivity field, with a vertical correlation length more than 16
351 times larger than the thickness of the domain, these simulations are effectively two-dimensional.
352 The results of these simulations are plotted in Figures 8 and 9. Figure 8 plots non-
353 dimensional outflow as a function of non-dimensional time for the three variances (lines with
354 filled symbols) for the three rainfall rates (increasing from the top to bottom) averaged over all
355 50 realizations. Also plotted are the corresponding base-case simulations with ε=0.01 (curves
356 with open symbols), the same curves shown in Figure 4. At the lowest rainfall rate (left panel)
357 both sets of simulations show a trend of increasing outflow with increasing $\sigma^2_{\ln K}$. The
358 statistically-anisotropic, base-case simulations predict more outflow than the statistically-
359 isotropic simulations, particularly at σ_f^2=5.0. At the intermediate rainfall rate, Q_{rain}/K_g=1.0, there
360 still is a trend of increasing outflow with increasing $\sigma^2_{\ln K}$, but with a much larger difference
361 between the statistically isotropic and anisotropic simulations in both the shape of the
362 hydrograph and the total flow. At the largest rainfall rate, a reversal in trend between the
363 statistically isotropic and anisotropic cases is observed. The base-case, with ε=0.01 predicts an
364 increasing runoff rate with increasing variance, while the statistically-isotropic case, with ε=1.0,
365 predicts the opposite behavior- decreasing outflow with increasing $\sigma^2_{\ln K}$.

366 Figure 9 confirms this behavior, plotting the percent total runoff as a function of variance
367 of *ln*(K) for the average of both cases (solid line) +/- one standard deviation (thin lines) with the
368 ε=1.0 case plotted with symbols. This figure also shows that the variance of the outflow behaves
369 differently for the two cases, particularly at the largest rainfall rate. In this figure we see that the
370 statistically anisotropic (i.e. 3D) cases produce greater runoff than the corresponding statistically
371 anisotropic (i.e. 2D) cases. These differences are quite significant at the greatest values of $\sigma^2_{\ln K}$
372 and for the largest rainfall rates. These differences underscore the contribution of processes such
373 as runon-generated excess infiltration and shallow perching. Exclusion of these important
374 processes could lead to significant errors in runoff estimation.

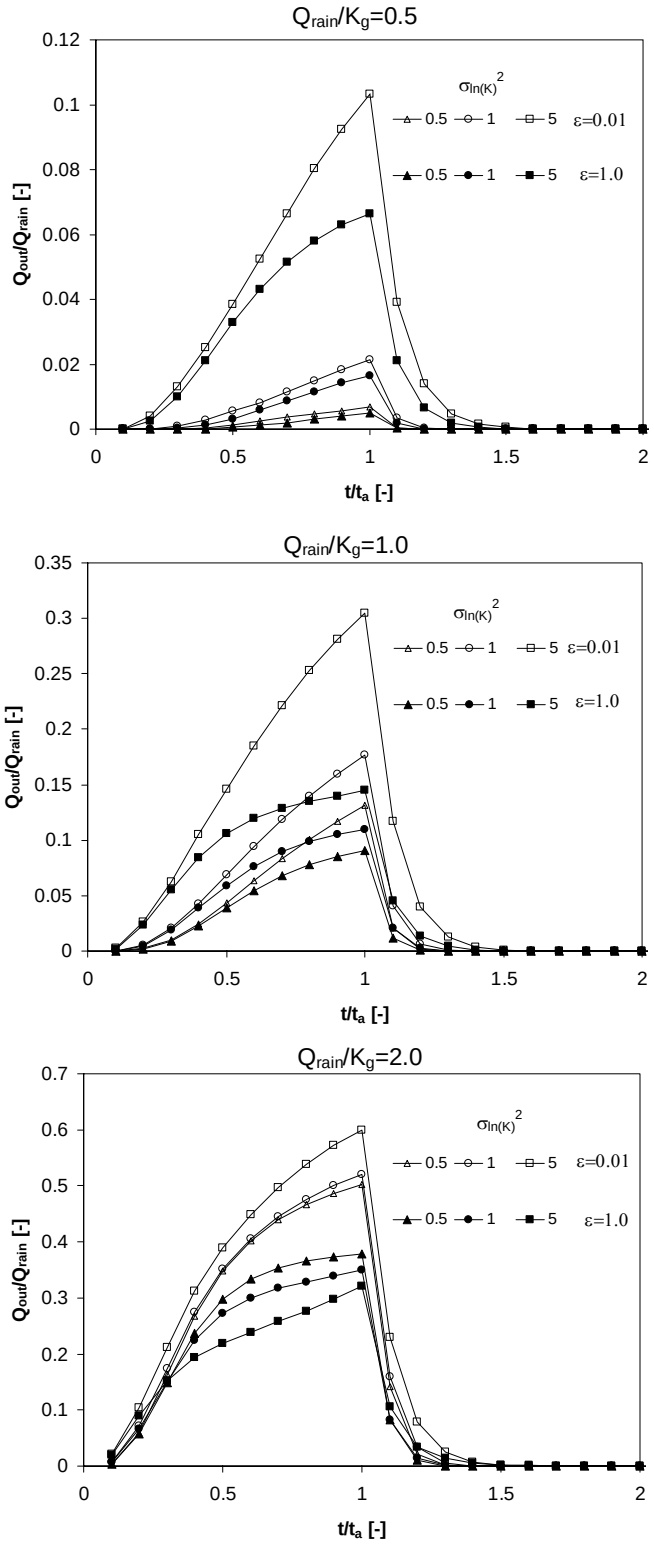

Figure 8. Plot of non-dimensional, ensemble-averaged outflow as a function of non-dimensional time for three variances (symbols as noted) for three non-dimensional rainfall rates (0.5, top to 2.0, bottom) for statistically isotropic (ε=1.0) and anisotropic (ε=0.01) cases. Note the difference in scale for the x-axis for the three figures.

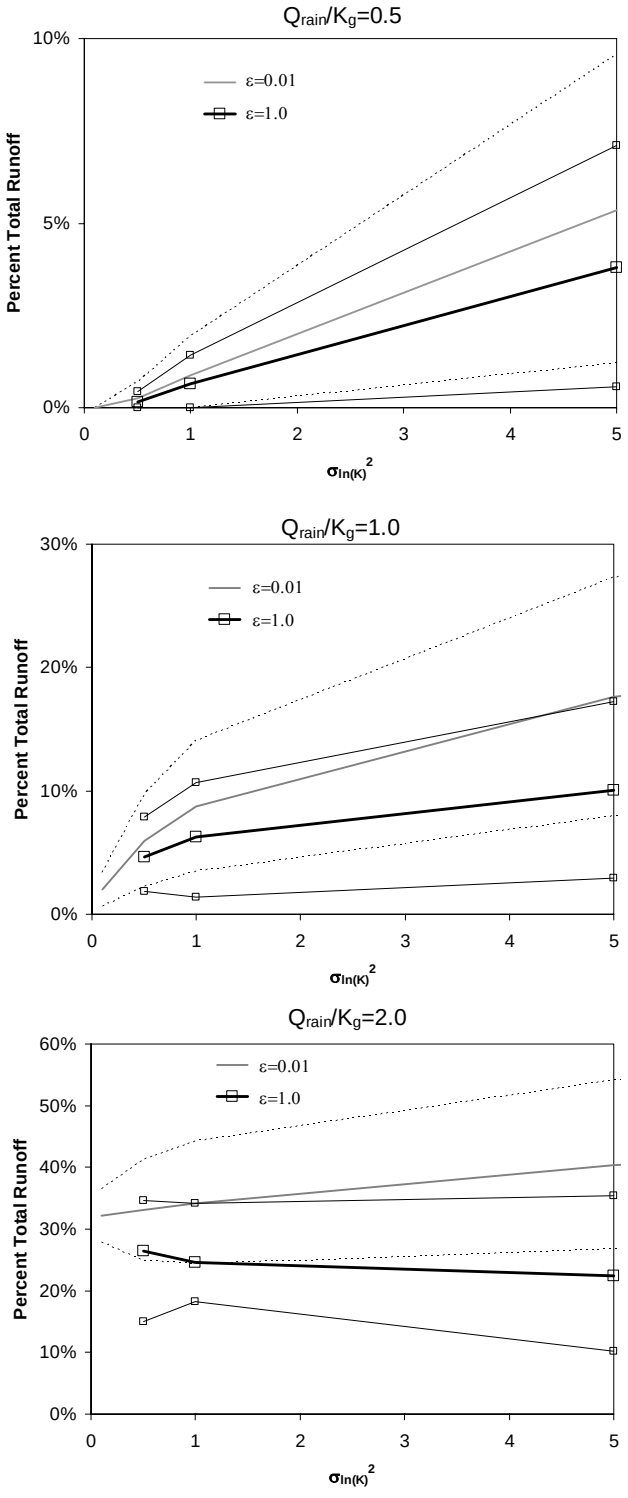

379

380 Figure 9. Plot of percent total runoff, averaged over all realizations (heavy lines) and +/- one standard deviation

381 (thin lines), as a function of variance of *ln*(K) for the statistically isotropic (ε=1.0, symbols) and anisotropic (ε=0.01,

382 solid lines). Note the difference in scale for the x-axis for the three figures.

Conclusions

We applied a fully coupled subsurface, overland flow model to examine Hortonian runoff in a simple hillslope with a heterogeneous subsurface. We investigate parametrically, the effects of a wide range of variance of *ln*K, normalized rainfall rates and statistical anisotropy. We also investigate ergodicity with several, very large domains, but only a single realization of hydraulic conductivity. Finally, we compare results of saturated area to some simple analytical tools for predicting excess infiltration areas. From these numerical experiments, we reach the following conclusions:

1. Three-dimensional subsurface heterogeneity, particularly vertical, structure in K_s, has a pronounced effect on Hortonian hillslope runoff. Statistical anisotropy in hydraulic conductivity produces trends in outflow with increasing $\sigma^2_{\ln K}$ that are the opposite of a statistically isotropic subsurface. Additionally, the runoff produced from the statistically isotropic cases was greater than the runoff produced from the corresponding isotropic cases.
2. Runoff/infiltration percentage varies greatly with rainfall rate and variance of *ln(*K), i.e. degree of heterogeneity.
3. An ergodic limit was determined to be around 30 integral scales but is only reached for larger rainfall rates with regard to the mean hydraulic conductivity.
4. The simple calculations of saturated area that might contribute to excess-infiltration generated runoff, based on hydraulic conductivity distributions at the land surface and rainfall rate, show poor agreement with the numerical simulations. Runoff parameterizations based upon these types of relationships would not be expected to produce accurate hydrographs.

While the inability of the simple relationships to predict saturated areas is discouraging, the ergodic behavior of the system for larger rainfall rates is not. This indicates that effective behavior might be reached at the hillslope scale. Analytic, stochastic approaches commonly applied to understand the role of subsurface heterogeneity on macrodispersion (e.g. Rubin and Dagan, 1992) might provide a template for understanding and upscaling Hortonian processes. In this manner, a new set of governing equations could be developed to represent small scale processes. Additionally, the changes in behavior shown in the presented numerical experiments should be used to guide field observations of hillslope runoff behavior. Coupling numerical experiments, theory and observations will yield a more complete understanding of the underlying processes.

Acknowledgements

This work was performed partially under the auspices of the U.S. Department of Energy by Lawrence Livermore National Laboratory under contract W-7405-Eng-48.

References

Ashby, S.F. and R.D. Falgout (1996). A parallel multigrid preconditioned conjugate gradient algorithm for groundwater flow simulations. *Nuclear Science and Engineering*, 124(1):145-59.

Binley, A., Elgy, J., Beven, K., (1989) A physically based model of heterogeneous hillslopes. 1. Runoff production. *Water Resources Research* 25 (6), 1219–1226.

Carle, S.F. and G.E. Fogg (1996) Transition probability-based indicator geostatistics, *Mathematical Geology*, 28(4): 453-476.

Carle, S.F. and G.E. Fogg (1997) Modeling Spatial Variability with One and Multidimensional Continuous-Lag Markov Chains, *Mathematical Geology*, 29(7): 891-918.

Dagan, G. (1989), *Flow and Transport in Porous Formations*, Springer-Verlag, New York.

Herbst, M., B. Diekkruger and J. Vanderborght (2006) Numerical experiments on the sensitivity of runoff generation to the spatial variation of soil hydraulic properties. *Journal of Hydrology*, 326: 43-58.

Kollet S.J. and RM Maxwell (2006) Integrated surface-groundwater flow modeling: a free-surface overland flow boundary condition in a parallel groundwater flow model. *Advances in Water Resources*, 29(7): 945-958.

Liang, X., E.F. Wood, D.P. Lettenmaier (1996), Surface soil parameterization of the VIC-2L model: Evaluation and modification. *Global and Planetary Change,* 13: 195-206.

Lohmann, D., E. Raschke, B. Nijssen and D.P. Lettenmaier (1998), Regional scale hydrology: I. Formulation of the VIC-2L model coupled to a routing model. *Hydrologic Science Journal*, 43:131-141.

Nahar, N., R.S. Govindaraju, C. Corradini and R. Morbidelli (2004) Role of runon for describing field-scale infiltration and overland flow over spatially variable soils. *Journal of Hydrology*, 286: 36-51.

Rubin, Y., and G. Dagan (1992) Conditional estimation of solute travel time in heterogeneous formations: Impact of transmissivity measurements, *Water Resources Research*, 28(4), 1033–1040.

Rubin, Y. (2003) *Applied Stochastic Hydrogeology* Oxford University Press.

Smith, L., and F. W. Schwartz, (1981) Mass transport, 2, A stochastic analysis of uncertainty in prediction, *Water Resources Research*, 17(2), 351–369.

Tompson, A. F. B., R. Ababou, and L. W. Gelhar (1989) Implementation of the three-dimensional turning bands random field generator, *Water Resources Research*, 25(10), 2227–2243.

Tompson, A. F. B., and L. W. Gelhar (1990) Numerical simulation of solute transport in three-dimensional randomly heterogeneous porous media, *Water Resources Research*, 26(10), 2541–2562.

Tompson, A. F. B., Falgout, R. D., Smith, S. G., Bosl, W. J., and Ashby, S. F. (1998), Analysis of subsurface contaminant migration and remediation using high performance computing: *Advances in Water Resources*, 22(3): 203-221

Wetzel, P.J., X. Liang, P. Irannejad, A. Boone, J. Noilhan, Y. Shao, C. Skelly, Y. Xue, Z-L Yang (1996), Modeling vadose zone liquid water fluxes: Infiltration, runoff, drainage, interflow. *Global and Planetary Change,* 13: 57-71.